UV-cured self-healing gel polymer electrolyte toward safer room temperature lithium metal batteries

Electrochimica Acta 433 (2022) 141265

Contents lists available at ScienceDirect

Electrochimica Acta

journal homepage: www.journals.elsevier.com/electrochimica-acta

UV-cured self-healing gel polymer electrolyte toward safer room temperature lithium metal batteries

Simone Siccardi [a], Julia Amici [a,*], Samuele Colombi [b], José Tiago Carvalho [c], Daniele Versaci [a], Eliana Quartarone [b], Luis Pereira [c], Federico Bella [a], Carlotta Francia [a], Silvia Bodoardo [a]

[a] Electrochemistry Group, Department of Applied Science and Technology, Politecnico di Torino, C.so Duca degli Abruzzi 24, Torino 10129, Italy
[b] Department of Chemistry, University of Pavia, Via Taramelli 16, Pavia 27100, Italy
[c] CENIMAT/i3N Department of Materials Science NOVA School of Science and Technology NOVA University Lisbon (FCT-NOVA) and CEMOP/UNINOVA Campus de Caparica, Caparica 2829-516, Portugal

A B S T R A C T

Solid polymer electrolytes are considered a useful solution for improving the safety of lithium metal batteries. However, these macromolecular systems show low ionic conductivity and suffer from limited cyclability at room temperature. In this work we propose the UV-induced, solvent-free radical copolymerization of poly (ethylene glycol) methyl ether methacrylate (PEGMEM, MW 500) and 2-(3-(6-methyl-4-oxo-1,4-dihydropyrimidin-2-yl)ureido)ethyl methacrylate (UpyMa) in the presence of poly(ethylene glycol) diacrylate (PEGDA, MW 575), used as crosslinker. The polymers, after activation in small amount of liquid electrolyte, show high thermal resistance, good lithium-ion conductivity and wide electrochemical window. Moreover, thanks to the quadruple hydrogen bond interaction of UpyMa dimer, the polymers show good self-healing properties both at 50 °C and room temperature. Such prepared polymers possess excellent interfacial stability and allow for stable lithium plating and stripping at room temperature. Last but not least, cycling tests against LFP cathode showed a fair and stable discharge capacity at 0.2C with 80% of capacity retention after 300 cycles. Most importantly, after severely mechanically damaging the electrolyte, it showed great recovery of the electrochemical properties, with a restored capacity of 115 mAh g^{-1} at 0.2C and room temperature. This work highlights a promising strategy for safer room-temperature self-healing quasi solid-state lithium metal batteries.

1. Introduction

Thanks to its high theoretical capacity (3860 mAh g^{-1}) [1] and low electrochemical potential (-3.04 V versus standard hydrogen electrode) [2], lithium metal anode represents a promising solution for energy storage challenges [3]. However, lithium anode suffers from dendrite formation [4], that can cause short circuit of the cell. Dendrites are uncontrolled structures formed during lithium plating process, from the uneven deposition of the metal [5]. Indeed, lithium can generate different structures (as, for example, mossy, granular, branched [6]), causing rupture of the solid electrolyte interphase (SEI), consuming electrolyte solution and, eventually, short circuiting the cell [7]. Moreover, most liquid electrolytes used in lithium metal batteries contain flammable solvents, causing additional safety issues in case of cells failing. For these reasons, solid polymer electrolytes (SPEs) have been widely studied in lithium metal batteries (LMBs) [8–10]. In this context, polymers containing polyethylene oxide (PEO) are the most reported [11], thanks to their good stability against metallic lithium [12,13] and to their ability to efficiently transport lithium cation through segmental motion of ethoxy-group rich polymer chains [14]. Other polymers reported in SPE application are poly(vinyl alcohol) [15,16] and polyacrylonitrile [17,18]. However, cells containing SPEs often suffer from low ionic conductivity as well as high interfacial resistance at room temperature, thus hindering their cycle life [19] and performances [20–22]. One solution envisioned to solve these issues is to activate the polymer membranes with small amounts of liquid electrolytes, thus obtaining the so-called gel polymer electrolytes (GPEs) [23,24]. Current GPEs are generally composed of polymer matrix, Li salt and organic solvents in a gel state and exhibit remarkable properties such as wide electrochemical window, good compatibility with both Li anode and common cathodes, high ionic conductivity since they have both the cohesive properties of solids and the diffusive transport properties of liquids in their unique hybrid network structure [25]. Some basic requisites for suitable polymer matrices include low glass transition temperature, fast segmental motion and the ability to dissociate the Li salts, these last require having large anions and low dissociation energy [26]. Moreover, the incorporation of plasticizers enhances ion dissociation, which implies a larger number of charge carriers for ionic transport in

* Corresponding author.
E-mail address: julia.amici@polito.it (J. Amici).

https://doi.org/10.1016/j.electacta.2022.141265
Received 5 August 2022; Received in revised form 20 September 2022; Accepted 27 September 2022
Available online 28 September 2022

addition to reducing the crystalline content while increasing the polymer segmental mobility of the polymer matrix [27]. GPEs with different polymer-solvent combinations have been studied in the last years and have demonstrated to both limit the liquid electrolyte evaporation and significantly reduce lithium dendrites formation [28]. Focusing on this last objective, the GPE polymer matrix should present sufficient mechanical properties to avoid lithium dendrites nucleation and growth, which is usually obtained by reticulated polymers through the use of crosslinkers [29]. However, another important factor has to be kept in mind: if the polymer interface with lithium is damaged either because of dendrites or other causes, this surface inhomogeneity will create preferential sites for additional dendrites nucleation and growth [30]. For this reason, scientists have ultimately focused their attention on new generation of materials with self-healing capability [31–33]. In general, self-healing materials have attracted significant attention over the past few decades due to their abilities to autonomously repair after a damage [34,35], more importantly their importance for the battery field was highlighted by the Battery2030+ Roadmap [36]. With this feature, a self-healing polymer electrolyte (SHPE) could indeed hinder dendrite formation [37], thus increasing cells safety and life cycle [38]. Different strategies have been introduced in the literature for creating self-healing polymers, through the use of different chemical bonds. Common examples are Diels-Alder reaction [39], ionic interaction [40–42], boronic esthers [43], metal ligand complexes [34] and cyclodextrins host-guest interaction [44]. In addition, great interest has been generated by hydrogen bond self-healing polymers [45,46] as they represent an easier implementation through a large family of molecules, like for example polyurethanes [47], and can self-repair without external stimuli [48]. In this context, polymers containing 2-(3-(6-methyl-4-oxo-1,4-dihydropyrimidin-2-yl)ureido)ethyl methacrylate [48–51] (UpyMa) are of great relevance thanks to the ability of ureidopyrimidinone to use a quadruple hydrogen bonding to form self-complementary dimers. In addition, this molecule can be easily methacrylated (obtaining UpyMa), thus allowing a simple polymerization technique with other acrylated/methacrylated monomers or polymers to prepare a self-healing macromolecular matrices [50,52].

In this work, we report the preparation of UpyMa through coupling reaction, followed by its copolymerization with poly(ethylene glycol) methyl ether methacrylate (PEGMEM) and poly(ethylene glycol) diacrylate (PEGDA) via a very quick and simple, one shot, solvent free, photo-induced radical polymerization.

The self-healing behavior of the obtained membranes was accurately assessed at 50 °C as well as at room temperature. Successively, full electrochemical characterization was performed, demonstrating the good thermal stability of the samples, their electrochemical stability against lithium and their ability to allow smooth lithium plating and stripping at a current density as high as 1 mA cm^{-2}. Last but not least, the membrane containing 5 wt% of UpyMa, with a lithium anode and a LFP cathode, was able to perform more than 300 cycles at 0.2 C at room temperature with capacity retention of 80%.

2. Experimental section

2.1. Materials

Poly(ethylene glycol) methyl ether methacrylate (PEGMEM, MW 500), poly(ethylene glycol) diacrylate (PEGDA, MW 575), 2-isocyanatoethyl methacrylate (ICEMA), methyl isocytosine (MIS), chloroform ($CHCl_3$), hexane, N-methylpyrrolidone (NMP), NaCl, Na_2SO_4 and dimethyl sulfoxide (DMSO) were purchased from Sigma-Aldrich and stored at 5 °C. All the chemicals were degassed in the prechamber for 5 min before being placed into the glove box to remove any residues of O_2 and H_2O.

After being synthesized, UpyMa was kept at room temperature and, before being used, was placed in oven at 70 °C to remove residues of $CHCl_3$. Then, it was transferred into the glove box for the preparation of the membranes.

2-hydroxy-2-methyl-1-phenyl-propan-1-one (Darocur) was purchased from Sigma-Aldrich and kept at room temperature in the glove box to avoid any interaction with atmospheric O_2.

2.2. Preparation of UpyMa

Synthesis of UpyMa was performed by addition organic reaction with ICEMA and MIS, as reported by Long et al. [53]. DMSO and MIS were mixed to create a 1.6 M solution in a flask. The flask was then placed in an oil bath under stirring and heating up to 170 °C with a magnetic stirrer. After that, the solution was removed from the oil bath and ICEMA was added in the flask. The MIS:ICEMA molar ratio was 1.0:1.1. After the addition of the ICEMA, the flask was immediately collocated in a water bath to cool down the solution at room temperature. At this time, the reaction product (UpyMa) started precipitating in the flask. UpyMa was then washed twice with distilled H_2O and twice with hexane. Afterward, the white precipitate underwent an extraction process to remove DMSO. To this end, $CHCl_3$ and UpyMa were mixed to create a homogeneous solution. Successively, an oversatured acqueous NaCl solution was added into the solution. When the two phases became separated, Na_2SO_4 was added to absorb the remaining H_2O in $CHCl_3$ solution. Eventually, $CHCl_3$ was separated from UpyMa with a Rotavapor. The yield of the reaction was 92.3%.

2.3. Preparation of UpyMa based membranes

UpyMa-based membranes were obtained by UV-induced radical polymerisation without using any organic solvent. The two oligomers PEGMEM and PEGDA were mixed in the fixed weight proportion 85:15, UpyMa was then added to this precursor solution in different proportions (namely 5 wt% and 10 wt% with respect to the precursor solution). All the formulations were prepared in glove box, under argon atmosphere (MBraunLabstar, O_2 rate <0.5 ppm; H_2O <0.5 ppm) to avoid O_2 inhibition. After 20 min of magnetic stirring in a vial, a white homogeneous solution was obtained. Then, Darocur was added in the proportion of 0.01 wt% with respect to the oligomers content and the solution was stirred for other 2 min. Afterward, the solution was casted on a support by doctor blade and irradiated under a UV lamp (wavelength emission peak: 365 nm) for 7 min. The supports used for UV-curing were either glass-slide or directly lithium metal. In the first case, the white polymer was peeled off the glass-slide and remained perfectly self-standing. The self-standing membranes had a thickness of ≈100 μm, while the ones prepared directly onto lithium showed a thickness of ≈80 μm. Last but not least, obtained membranes were activated by swelling for 15 min in commercial liquid electrolyte (purchased from Solvionic). The liquid electrolyte chosen was $LiPF_6$ 1.0 M in 1:1 v/v mixture of ethylene carbonate (EC) and diethylene carbonate (DEC). From now on, the membranes prepared with 5 wt% UpyMa will be referred to as PPU5 and the ones prepared with 10 wt% UpyMa as PPU10.

2.4. UpyMa and membranes characterization

Samples morphologies were examined using a field emission scanning electron microscope (FESEM, TESCANS9000G). ^1H nuclear magnetic resonance (NMR) spectra were recorded on a Bruker 200 MHz instrument, calibrated with the solvent residual proton signal for the UpyMa characterization ($CHCl_3$ was dried using 4 Å molecular sieves). ^1H NMR spectra of membranes were recorded on Bruker 400 MHz instrument and calibrated with the solvent residual proton signal (deuterated DMSO is used as solvent). Thermal stability was assessed through thermo-gravimetric analysis (TGA) performed in air, between 25 and 800 °C at 10 °C min^{-1} on a NETZSCH TG 209F3 instrument. Effective cross-linking was checked through Fourier transform infrared spectroscopy (FTIR), on a NicoletTM iS50 FTIR spectrometer (Thermo

Scientific TM) equipped with an attenuated total reflection tool over the range 4000-400 cm^{-1} with a resolution of 4 cm^{-1} at room temperature. Optical images of the polymer samples were obtained by an optical stereoscope Leica M80. Scanning electron microscopy (SEM) images of the polymer samples were performed by SEM Hitachi TM 3030Plus Tabletop, operated at 15 kV. The liquid electrolyte uptake (*LEU*) was obtained by measuring the weight of the dry membrane and the saturated membrane after immersion for 18 h in the electrolyte. The electrolyte uptake was calculated according to Eq. (1).

$$LEU = ([M_e - M_0] / M_0)\text{x}100 \quad (1)$$

where M_0 and M_e are the weights of the membrane before and after immersion, respectively.

2.5. Cathode preparation

The LFP cathode was prepared by tape casting the homogeneous slurry of $LiFePO_4$ (purchased from Aleees), Carbon C65 (Imerys) and poly(vinyledenfluoride) (Arkema Kynar 761) (w/w/w = 70/20/10) in NMP on an Al foil. Then, the electrode was dried at 50 °C for 1 h and kept at room temperature overnight. The typical active mass loading was 1.5 mg cm^{-2}. The as-obtained electrode was cut into 15 mm diameter discs and dried under vacuum at 120 °C for 4 h.

2.6. Electrochemical characterization

To determine the ionic conductivity (σ) of the membranes, electrochemical impedance spectroscopy (EIS) of the samples, sandwiched between two stainless steel (SS) blocking electrodes, were carried out on an electrochemical workstation (CHI660D). The frequency of the EIS test ranged from 1 to 10^5 Hz with an amplitude of 10 mV. The measurements were performed between and 20 and 60 °C, with a 10 °C step. The ionic conductivities were calculated at each temperature using Eq. (2):

$$s = (l / A) * (1 / R_W) \quad (2)$$

where l, A and R_Ω represent the thickness of the membrane, the membrane surface area and its resistance, measured at the high-frequency intercept on EIS spectra, respectively.

The electrochemical stability window was evaluated by linear sweep voltammetry (LSV), performed between 1 and 5.5 V *vs.* Li^+/Li, on asymmetrical SS/Membrane/Li cells. The measurements were performed on an electrochemical workstation (CHI660D) at a scan rate of 0.2 mV s^{-1} at room temperature.

The interfacial stability of the prepared membranes against lithium was studied at open circuit voltage (OCV) by EIS on an electrochemical workstation (CHI66OD) through Li/Membrane/Li symmetric cells. The frequency of the EIS ranged from 0.01 to 10^5 Hz with an amplitude of 10 mV.

The Li-ion transference number (t_{Li+}) was investigated by a potentiostatic polarization method using a symmetrical Li/Membrane/Li symmetric cell. The Li-ion transference number t_{Li+} can be calculated following Eq. (3):

$$t_{Li+} = [I_s \times (\Delta V - I_0 R_0)] / [I_0 \times (\Delta V - I_s R_s)] \quad (3)$$

where I0 and IS are the initial and steady-state current values, respectively. ΔV is the applied DC potential (10 mV); R0 and R_S are the interfacial impedance values at initial and steady state, respectively [54].

To assess the influence of the membrane on lithium plating and stripping, galvanostatic cycling was carried out at different current densities on Li/membrane/Li symmetrical cells.

The lifetime and the rate capability were studied by galvanostatic charge/discharge tests at different C-rates on Li/Membrane/LFP cells by an Arbin Instruments equipment. The potential window was 2.5 – 4.2 V *vs.* Li^+/Li and the C-rates were defined on the basis of LFP cathode standard specific capacity of 170 mAh g^{-1}.

To verify the operative self-healing behavior a cell with lithium metal anode and LFP cathode was cycled at 0.2C for 10 cycles before being stopped and opened, in order to cut the SHPE. Afterwards, the cell was closed again, left to rest for 12 h at room temperature and the cycling was resumed at 0.2C. As a mean of comparison, a cell with a Celgard separator was subjected to the same protocol.

All the previously described cells were assembled in ECC-Std test cells (EL-CELL GmbH, Germany) in an argon-filled glovebox.

3. Results and discussion

3.1. UpyMa characterization

UpyMa was obtained by a coupling reaction from ICEMA and MIS; the chemical structure of the obtained molecule was characterized by NMR and FTIR analyses.

NMR spectra of ICEMA, MIS and UpyMa are reported in Fig. 1a, confirming that the synthesized sample presents the typical NMR peaks described in literature [48,55]. In comparison with MIS and ICEMA NMR spectra, a new characteristic peak is present in UpyMa at 10.5 ppm, corresponding to the H-N of new ureido group of UpyMa. Moreover, the absence of the peak at 6.5 ppm, corresponding to the amidic group of MIS, demonstrates the complete utilisation of the reactant in the synthesis. The typical peaks of ICEMA (described with orange, red, blue and green points in Fig. 1a) are all present in UpyMa spectrum, with the exception of the isocyanate ICEMA group that reacts during the process. Eventually, no peak typical of the solvents used is present in the UpyMa spectrum, confirming the successful purification. To further substantiate the assessment of the chemical structure, FTIR analysis was performed and the obtained spectrum for UpyMa is reported in Fig. 1b together with that of ICEMA. Typical peaks previously assigned to UpyMa [48] can be individuated in the spectrum. In particular, the characteristic stretching peaks at 1589 cm^{-1} and 1661 cm^{-1} are typical of the ureido group, synthesized in the coupling reaction. In comparison with the ICEMA spectrum, the disappearance of the peak at 2267 cm^{-1} in the FTIR spectrum of UpyMa, which corresponds to the vibration of ICEMA isocyanate group, further confirms the reaction completion [52].

3.2. Membranes characterization

Afterward, polymer membranes were prepared by UV-initiated radical copolymerization of PEGMEM, PEGDA and UpyMa, allowing to obtain highly crosslinked samples with UpyMa moieties. Two different contents of UpyMa were added to the precursor formulation, *i.e.*, 5 and 10 wt%, allowing to obtain the samples PPU5 and PPU10, respectively. Initially, FTIR characterization was performed to verify the successful crosslinking (Fig. 2a) in both cases.

The peaks at 1661 and 1589 cm^{-1} are typical of the C=O and C=C vibrations of the amidic group of UpyMa [48], respectively. The presence of such peaks in the FTIR spectra of the membranes confirms the copolymerization of UpyMa in the final polymer structure, thanks to its methacrylate group [48]. However, the obtained spectra do not clearly show the typical methacrylate peak situated around 1630 cm^{-1}, preventing any conclusion regarding its conversion during the crosslinking process. Therefore, ^{1}H NMR spectroscopy was performed in order to further investigate this aspect (see Fig. S1). The obtained spectra seem to confirm, in both cases the successful copolymerization. However, regarding PPU10 sample, the chemical shift corresponding to the methacrylate group shows a more pronounced peak than for the PPU5 sample, which might imply an incomplete copolymerization. Anyway, the intensity of such peak remains limited, suggesting that the conversion is almost complete.

Thermal stability represents a critical factor for safety performance

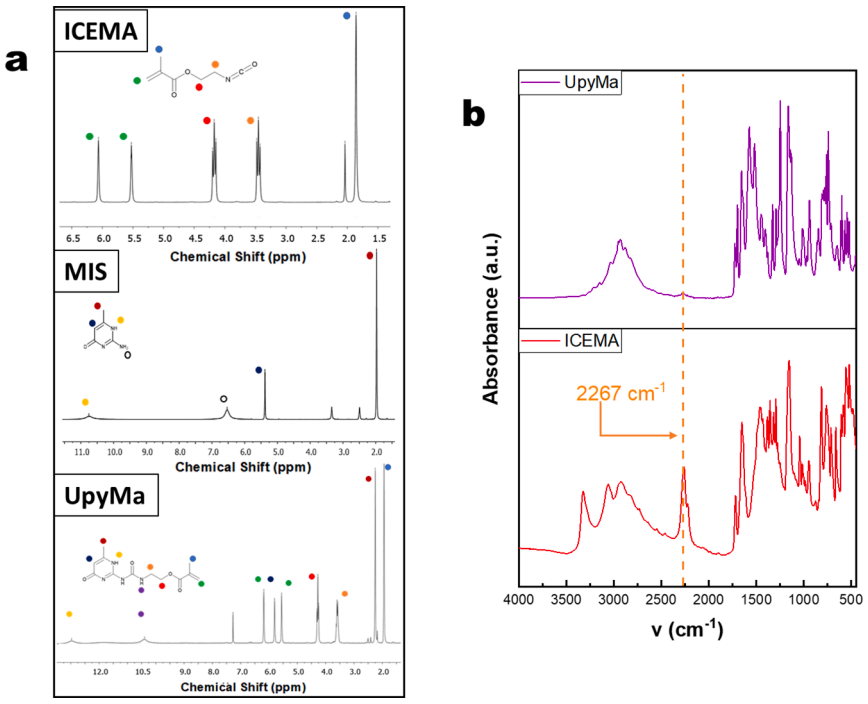

Fig. 1. (a) NMR spectra of ICEMA, MIS and UpyMa. (b) FTIR spectra of UpyMa and ICEMA.

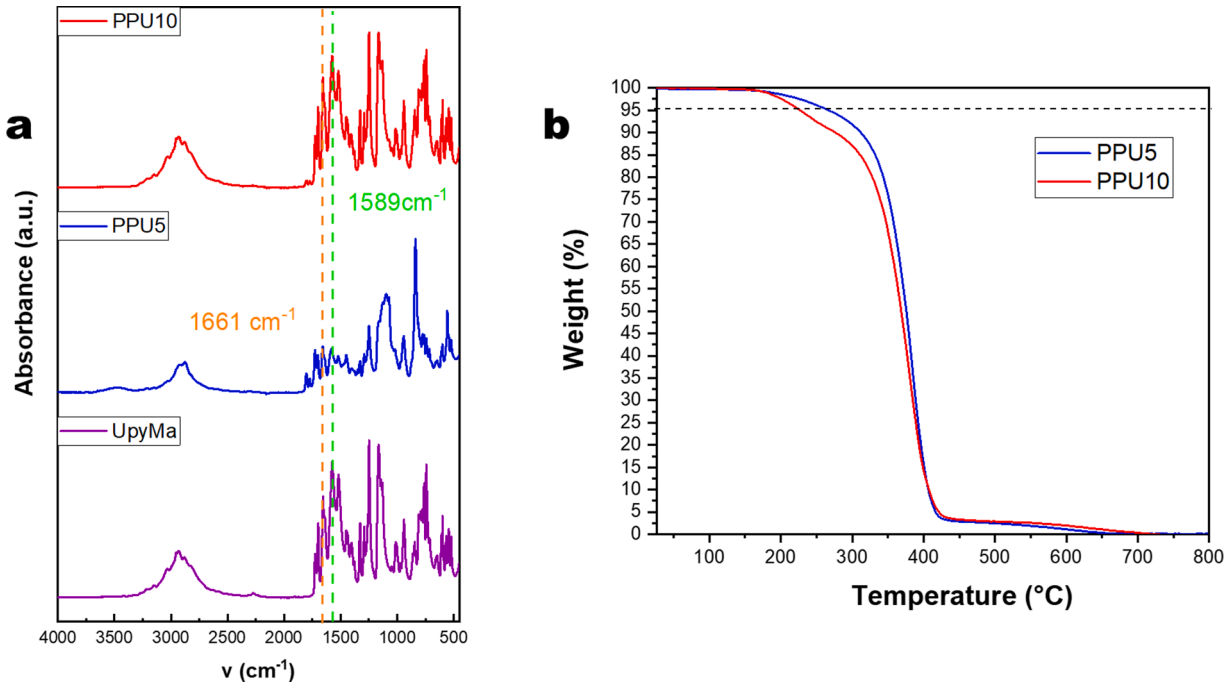

Fig. 2. (a) FTIR spectra of PPU10, PPU5 and UpyMa. (b) TGA curves of PPU5 and PPU10 samples.

of electrolytes for LMBs. To this purpose, TGA analyses were carried out on the UV-cured polymers (Fig. 2b). The two polymers were thermally stable up to 170 °C, which guarantees safe performances in the temperature range of operation typical of LMBs, making them suitable as SPEs. However, a small difference in the PPU10 profile can be noted at approximately 250 °C, which could be an additional hint of a partially incomplete copolymerization of UpyMa in PPU10.

Successively, the morphology of the two samples was studied by FESEM. Panels labelled from a) to f) in Fig. 3 show the morphological structure of the surface and cross section of PPU5 and PPU10 samples, respectively. Both membranes showed a homogenous surface, in addition the cross-section analyses (Fig. 3c and f) revealed the membranes thickness were around 115 μm and 131 μm for PPU5 and PPU10, respectively. The enlarged magnification FESEM micrographs (Fig. 3b and 3e) reveal a wave structure of the surface of the membranes. An explanation could be UpyMa groups interactions thanks to H-bond on the surface of the samples. To better understand this feature, surface energy dispersive spectroscopy (EDS) analysis was carried out. Since UpyMa is the only material containing nitrogen, EDS can be used to determine the distribution of UpyMa molecules on the surface of the

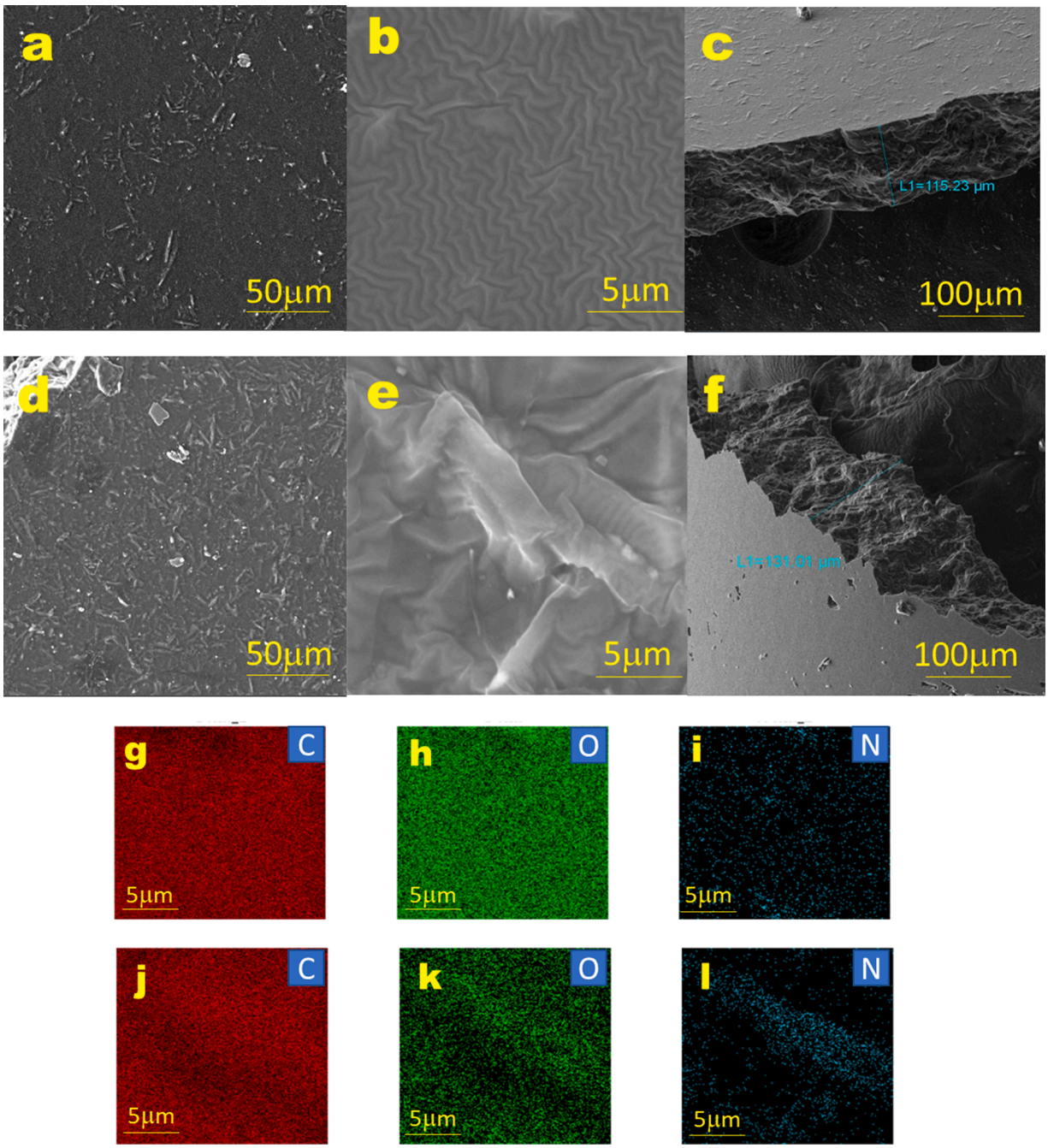

Fig. 3. FESEM micrographs of (a) PPU5 surface at low magnification, (b) PPU5 surface at high magnification, (c) PPU5 cross-section, (d) PPU10 surface at low magnification, (e) PPU10 surface at high magnification, (f) PPU10 cross-section. EDS analysis PPU5 showing (g) carbon, (h) oxygen and (i) nitrogen elements. EDS analysis of PPU10 showing (j) carbon, (k) oxygen and (l) nitrogen elements.

polymer. Fig. 3i and 3l show the results of the EDS analysis, proving that nitrogen is homogeneously distributed on the surface of the membranes and further confirming the successful preparation of homogeneous co-polymers containing UpyMa groups, through UV-induced radical polymerisation.

After carefully assessing the chemical structure and the thermal properties of the prepared samples, their self-healing capability was investigated. To this end, the membranes were cut with a cutter, then the two pieces were placed side by side and analysed with an optical microscope (Fig. 4 a and b, on the left) and by SEM (Fig. 4 c and d, on the left). Afterward, the cut polymers were placed between two glass slides under a small pressure applied by paper clips and left at 50 °C for 2 h before assessing their morphology again (Fig. 4, right side). This test was repeated at room temperature (see Fig. S2). The two polymers demonstrated good self-healing ability either after 2 h at 50 °C (see Fig. 4, right-side) or overnight at room temperature (see Fig. S2). Indeed, both optical images and SEM micrographs show limited scar on the studied surface and the self-healed polymers could be easily peeled off the glass support. Such self-healing behavior is due to the dynamic quadruple hydrogen bonding interaction provided by UpyMa, as illustrated schematically on Fig. S3; in addition, this process can occur rapidly at 50 °C (2 h) but, more impressively, it can be verified also at room temperature, even if the time involved is longer. Last but not least, no significant difference in the self-healing behavior could be individuated between PPU5 and PPU10 samples.

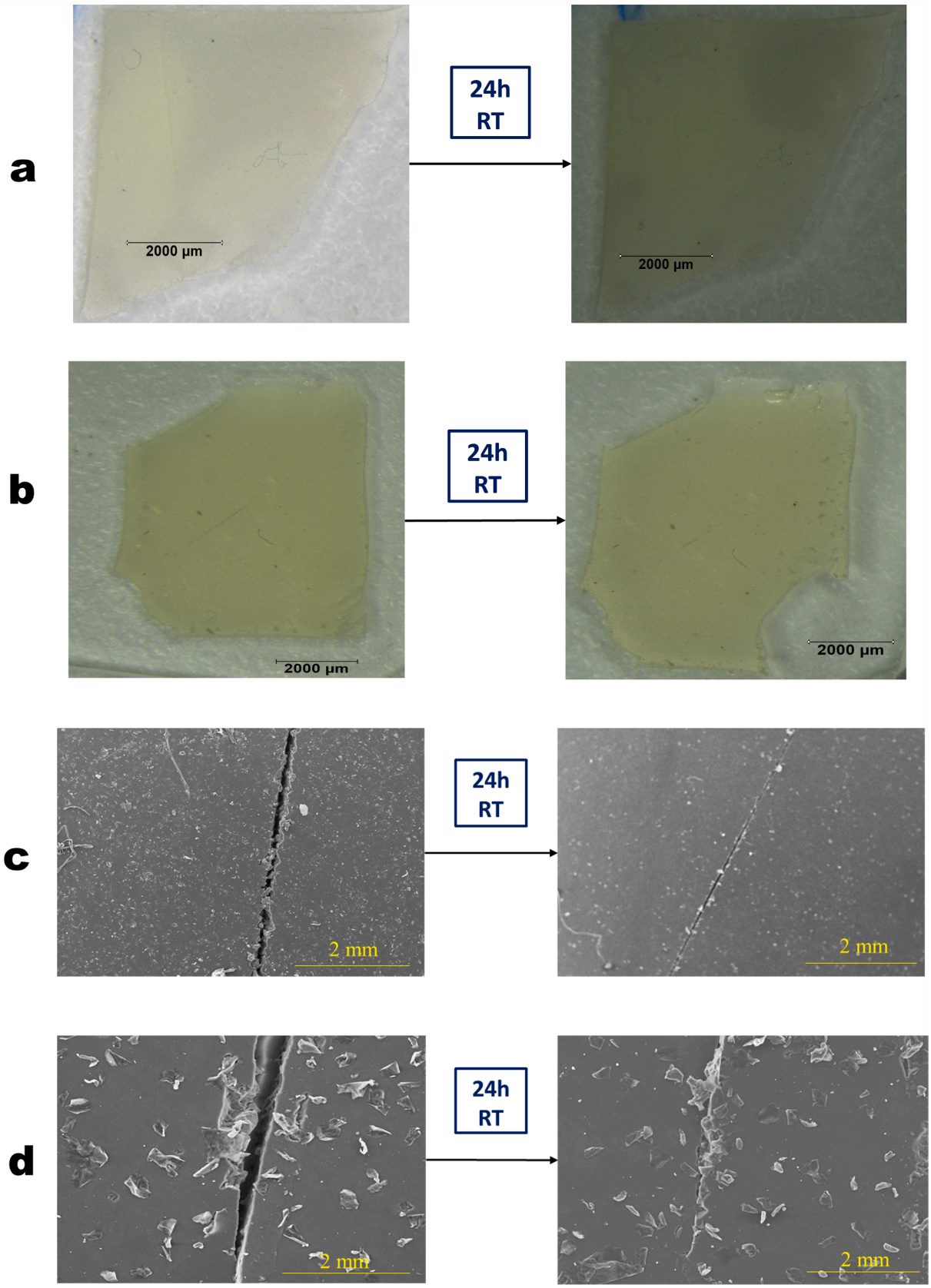

Fig. 4. Optical images of (a) PPU5 and (b) PPU10 samples between glass-slides, (left) before and (right) after self-healing process at 50 °C for 2 h. SEM micrographs of (c) PPU5 and (d) PPU10 samples (left) before and (right) after self-healing process at 50 °C for 2 h.

3.3. Electrochemical characterization

After addressing the morphological and structural characterization of the membrane along with the assessment of its self-healing properties, electrochemical characterization was carried out to further verify the suitability as electrolyte for LMBs.

Electrolyte uptake is an important parameter to verify the compatibility of the two polymers with the electrolyte solution, thus ensuring a proper ionic conductivity. The results obtained (see Table S1) show high capacity of the membranes to retain liquid electrolyte into their reticulated structure, with a slightly higher value for PPU10 compared to PPU5. The influence of such values was verified by measuring the ionic conductivities of both samples at different temperatures. Fig. 5a shows the plots of the ionic conductivity versus temperature for the two polymers from 20 to 60 °C. As expected, for the two membranes, conductivity increased by increasing the temperature. More surprisingly, the different contents of UpyMa and the consequent variation in LEU did not affect the polymers conductivity. In fact, both samples present comparably high values. In particular, the high ionic conductivity (1.88×10^{-3} S cm^{-1}, for PPU5) at room temperature confirms the suitability of the PPU membranes as SHPE for lithium metal cells.

Electrochemical stability, particularly at high potentials, is another crucial parameter for this application, therefore LSV was performed at room temperature on PPU5 (Fig. 5b) and PPU10 (Fig. S4) samples. The profiles obtained on both cases look very similar, confirming the electrochemical stability of both samples up to 5.0 V.

Another important parameter when dealing with Li metal anode is interfacial stability. To investigate the interfacial behavior of PPU5 and PPU10, EIS was monitored in symmetrical cells at OCV for 30 days. Fig. 5c and d show the variation of the AC impedance with time. The impedance spectrum of PPU5 shows an initial charge transfer resistance at around 400 Ω, mainly explained by a poor initial contact with lithium and eventually the formation of a thin spontaneous SEI layer. Then, the charge transfer resistance decreases to 350 Ω and stabilises with time, confirming the absence of noticeable reactions between the sample and metallic Li. On the contrary, for PPU10 sample, the charge transfer resistance shows a constant increase with time, reaching a maximum value of 1800 Ω after 20 days. In this case, the membrane features less stable behavior against lithium, a possible explanation could be the presence of incompletely reacted methacrylate groups from UpyMa, as previously suspected. For this reason, PPU10 membrane was not further considered for characterization.

The Lithium-ion transference number (t_{Li+}) was assessed by performing chronoamperometry and EIS at room temperature on a symmetrical cell containing PPU5, as described in [54]. As shown in Fig. S5, the t_{Li+} calculated is 0.62. This high transference number value demonstrates the good Li ion diffusion in PPU5, which should avoid the formation of concentration gradient and consequent cell polymerization upon cycling, particularly at higher C-rate.

Formation of dendrites is a critical factor for LMBs, mainly because of dendrites nucleation and growth hindering cells specific capacity by dead lithium formation, in addition to the possibility of short-circuit leading to more hazardous events. Therefore, lithium plating stripping was performed on symmetrical cells containing PPU5 at room temperature and at a current density of 0.1 mA cm^{-2} with a fixed capacity of 0.1 mAh cm^{-2}. The first 30 cycles, reported in Fig. 6a, show that the cell containing PPU5 presents a stable profile, with a relatively low polarization. The same test was repeated in more drastic conditions, namely 1 mA cm^{-2} with a fixed capacity of 1 mAh cm^{-2} at room temperature. The results were compared to a symmetric cell assembled with Celgard 2500 separator activated with the liquid electrolyte and tested following the same procedure; the profiles are reported in Fig. S6. On the first cycles, both cells present severe fluctuations, with a large voltage polarization, implying Li dendrite growth on the Li metal surface. However,

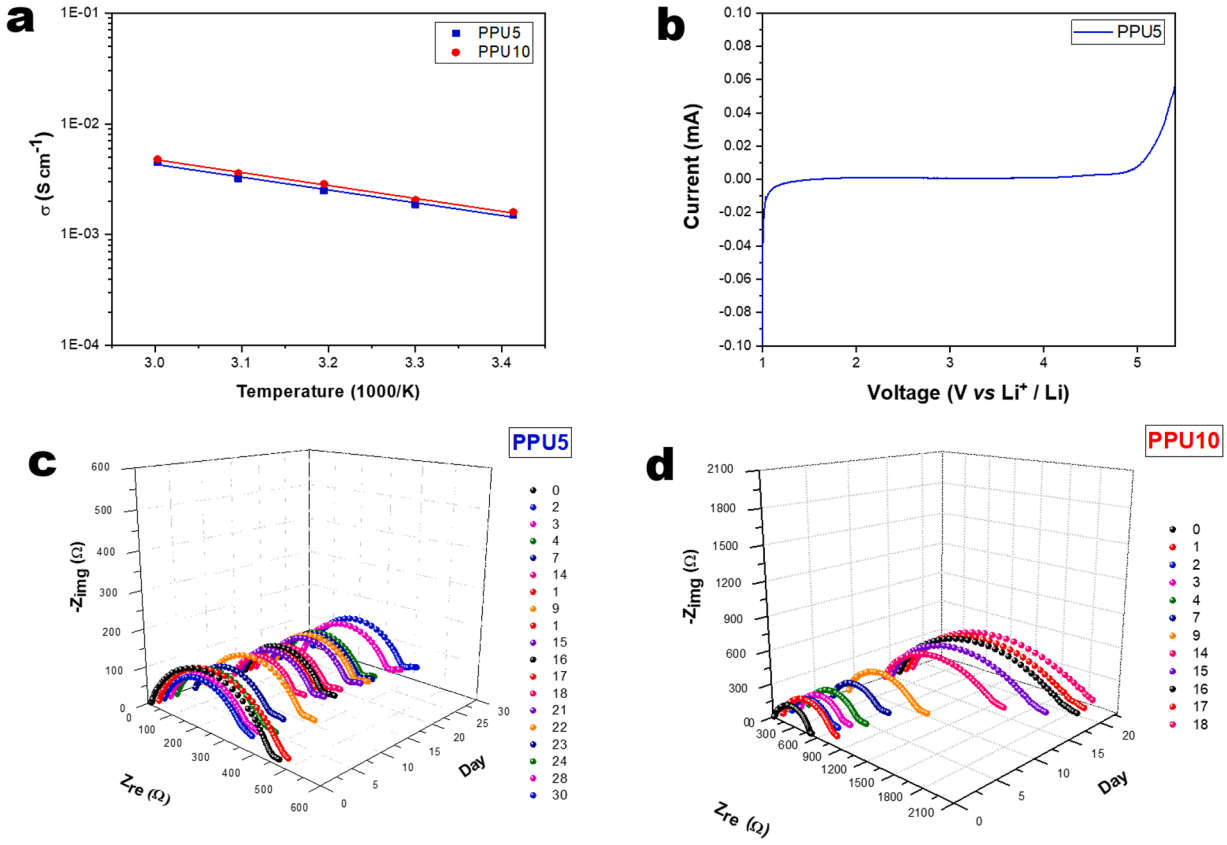

Fig. 5. (a) Temperature dependence of ionic conductivity for PPU5 and PPU10 samples. (b) LSV plot of a Li/PPU5/SS cell at room temperature. (c) Interfacial stability assessed by a Li/PPU5/Li cell at room temperature. (d) Interfacial stability assessed by a Li/PPU10/Li cell at room temperature.

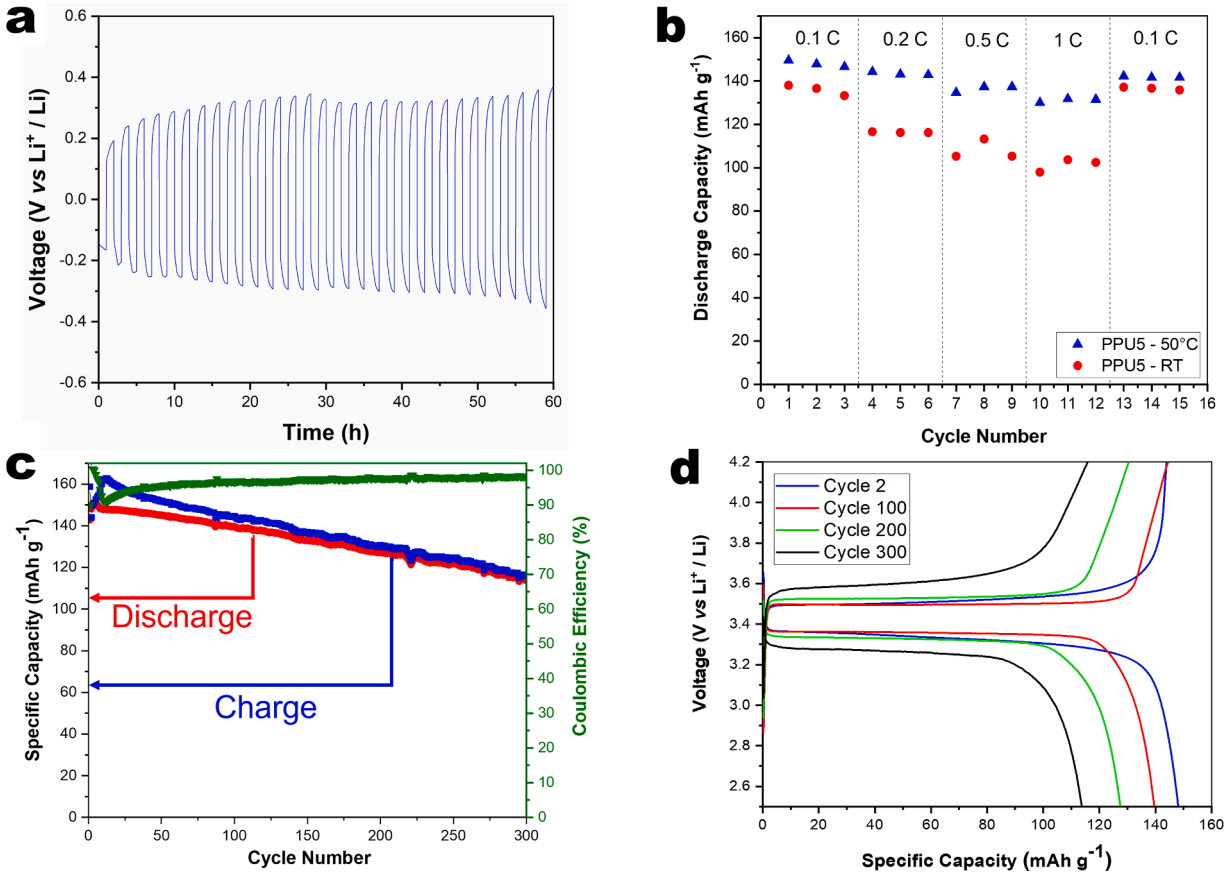

Fig. 6. (a) Lithium plating and stripping results of the Li/PPU5/Li symmetrical cell at a current density of 0.1 mA cm^{-2} and at a fixed capacity of 0.1 mAh cm^{-2}, at room temperature. (b) Rate capability test of a Li/PPU5/LFP cell at 50 °C and at room temperature. (c) Cycling performance of the Li/PPU5//LFP cell at 0.2C at room temperature. (d) Charge and discharge curves of the Li/PPU5/LFP cell at 0.2C, carried out at room temperature.

interestingly, while the Celgard cell profile clearly shows a short-circuit after ≈50 h, the PPU5 cell was able to keep cycling for more than 600 h with a more stable profile and without short-circuiting. This result demonstrates the ability of PPU5 as SHPE to limit dendrites formation and avoid short-circuits, probably thanks to its highly cross-linked structure and self-healing capability.

The cycling performance of PPU5 in a lithium metal cell was tested against a LFP cathode. Rate capability tests are reported in Fig. 6b, with PPU5 membrane sandwiched between the Li anode and the LFP cathode, at two different temperatures (*i.e.*, RT and 50 °C). As expected, the cell shows better electrochemical behavior at 50 °C, due to the enhanced ionic conductivity in the polymer matrix. Nevertheless, PPU5 also shows very good C-rate performance at room temperature. In fact, at 1C, the cell delivers a discharge capacity as high as 100 mAh g^{-1}. Moreover, the cell recovers its initial capacity going back to 0.1C, that is 140 mAh g^{-1}. These results are quite impressive in the case of a GPE-based cell studied at room temperature.

To further assess long cycling performances of such cell at room temperature, galvanostatic cycling was performed at 0.2C. The cell demonstrated an initial discharge capacity as high as 143 mAh g^{-1} (Fig. 6c). In the meantime, for the first cycles the charge capacity slightly overcame the discharge one; this could be explained by cell formation as well as some parasitic reactions caused by the SEI layer formation. However, such phenomenon fades away after the initial cycles, allowing the cell to reach 100% Coulombic efficiency and remaining stable, as it reached the 300th cycles with a 98% Coulombic efficiency. In terms of discharge capacity, 114 mAh g^{-1} was retained after 300 cycles, corresponding to a noteworthy capacity retention of 80%. Therefore, the capacity loss is around 0.07% per cycle, which is very limited and could be ascribable to some liquid electrolyte decomposition relative to the SEI evolution. Such hypothesis is partially confirmed by post-mortem FESEM analysis of the PPU5 membrane after 300th dis-/charge cycles in the Li/PPU5/LFP cell (Fig. 7Sa) showing no obvious sign of membrane degradation. Similarly, no substantial changes in the values of the charge transfer resistance are observed before and after cycling by EIS analysis (Fig. 7Sb). The EIS spectra of the Li/PPU5/LFP cell before and after 300th cycles demonstrate the stable behavior of PPU5 for the entire operational life of the cell tested in this work.

As already mentioned, lithium reactivity is an issue for LMBs, as the inhomogeneous redeposition upon cycling tends to create 3D structures which can then break, hence loosing contact with the anode, and form a layer of the so-called dead lithium. Such layer represents an obstacle to Li^+ diffusion and cell reactions in general, which results in constant increasing of the cell overvoltage. Interestingly, as can be observed in Fig. 6d, though our cell was cycled at room temperature, no significant increase in the cell overvoltage could be noted for the first 200 cycles, preserving the typical discharge and charge voltage plateau of LFP. Moreover, even after 200 cycles and up to the 300th, the increase resulted very limited.

Eventually, to further demonstrate the PPU5 self-healing capability, a cell with lithium metal anode and LFP cathode was cycled at 0.2C for 10 cycles before being opened, in order to cut the SHPE. Afterwards, the cell was closed again, left to rest for 12 h at room temperature and the cycling was resumed at 0.2C. As can be seen in Fig. 7a, PPU5 managed to self-repair after the cut and resume cycling with minimum capacity fade, with a restored capacity of 115 mAh g^{-1}. Moreover, Coulombic efficiency was also retained before and after cutting. The same procedure was followed with a commercial Celgard 2500 separator impregnated with the liquid electrolyte. As seen in Fig. 7b, the cell capacity drastically collapsed after cutting. FESEM analysis of PPU5 at the end of this

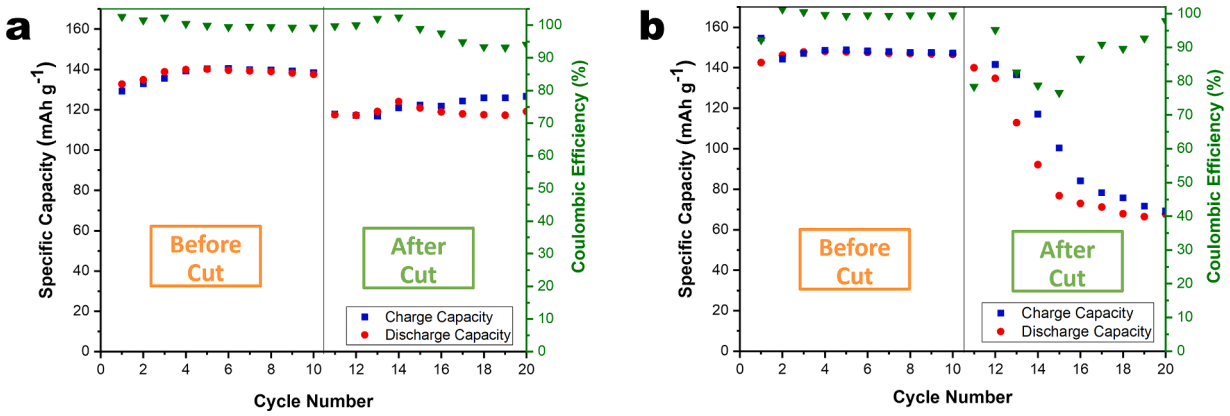

Fig. 7. (a) Cycling performance of a Li/PPU5/LFP cell at 0.2C and room temperature before and after cutting the PPU5 membrane. (b) Cycling performance of a Li/Celgard 2500/LFP cell at 0.2C and at room temperature before and after cutting the Celgard 2500 membrane.

cycling test, reported in Fig. S8, shows that the membrane morphology after cutting and cycling again is quite similar to the pristine one (Fig. 3b), with the presence of limited scars on the surface. Such results demonstrate the ability of the membrane to self-repair and maintain cell performances, thus constituting a very promising step towards the preparation of self-healable LMBs. Table S2 reports a comparison between the PPU5 membrane synthesized in this work with similar SPE and GPE membranes reported in literature in terms of conductivity, self-healing properties, Li ion transfer number and electrochemical performances along with the synthesis conditions. The fast and easy synthesis and the good electrochemical performances obtained both at high current density and with long dis-/charge cycling at room temperature give the PPU5 membrane an interesting breakthrough in the use of self-healing polymers in metal battery application.

4. Conclusions

In summary, UpyMa was synthesized and characterized by NMR and FTIR techniques. Afterwards, two different formulations were prepared containing different weight ratios of UpyMa (*i.e.*, PPU5 and PPU10) crosslinked to methacrylate oligomers through UV-initiated radical polymerization without using any solvents. The two polymers showed good thermal stability and homogeneous surface morphology. Self-healing tests carried out on the polymers showed good self-repairing ability after damage under mild pressure at 50 °C and even at room temperature, thanks to the intermolecular dynamic H-bonding interaction of UpyMa in the polymer network. PPU5 and PPU10 samples showed high ionic conductivity, however PPU10 demonstrated a poor interfacial stability with Li and was therefore discarded. On the contrary, thanks to its good interfacial stability, homogeneous lithium plating and striping was obtained with PPU5, confirming that it could be a good candidate as SHPE in LMBs. Indeed, Li/PPU5/LFP cell showed a great performance with capacity retention of 80% after 300 cycles. Most importantly, after severely mechanically damaging the electrolyte, it showed great recovery of the electrochemical properties, with a restored capacity of 115 mAh g^{-1} at 0.2C and room temperature. This work demonstrates the importance of self-healing GPEs to increase long-term stability of Li metal cells for future safer and more performant batteries.

CRediT authorship contribution statement

Simone Siccardi: Methodology, Investigation, Data curation, Writing – original draft. **Julia Amici:** Conceptualization, Methodology, Writing – original draft, Writing – review & editing. **Samuele Colombi:** Methodology, Investigation. **José Tiago Carvalho:** Methodology, Investigation. **Daniele Versaci:** Conceptualization, Methodology, Writing – review & editing. **Eliana Quartarone:** Writing – review & editing. **Luis Pereira:** Writing – review & editing, Funding acquisition. **Federico Bella:** Writing – review & editing. **Carlotta Francia:** Writing – review & editing. **Silvia Bodoardo:** Writing – review & editing, Funding acquisition.

Declaration of Competing Interest

The authors declare that they have no known competing financial interests or personal relationships that could have appeared to influence the work reported in this paper.

Data availability

Data will be made available on request.

Acknowledgments

The Authors acknowledge the support from Portuguese Foundation for Science and Technology under the scholarship SFRH/BD/139225/2018 and financed projects CHIIHC (PTDC/NAN-MAT/32558/2017), and CELLECTIVE (PTDC/CTM-CTM/4653/2021). This work received funding from the European Union's Horizon2020 research and innovation program under grant agreement No: 952169 (SYNERGY project, H2020-WIDESPREAD-2020-5, CSA).

Supplementary materials

Supplementary material associated with this article can be found, in the online version, at doi:10.1016/j.electacta.2022.141265.

References

[1] Q. Li, S. Zhu, Y. Lu, 3D porous Cu current collector/Li-metal composite anode for stable lithium-metal batteries, Adv. Funct. Mater. 27 (2017), 1606422, https://doi.org/10.1002/adfm.201606422.
[2] N.W. Li, Y. Shi, Y.X. Yin, X.X. Zeng, J.Y. Li, C.J. Li, L.J. Wan, R. Wen, Y.G. Guo, A flexible solid electrolyte interphase layer for long-life lithium metal anodes, Angew. Chem. Int. Ed 130 (2018) 1521–1525, https://doi.org/10.1002/ange.201710806.
[3] Y. Bai, N. Muralidharan, Y.K. Sun, S. Passerini, M. Stanley Whittingham, I. Belharouak, Energy and environmental aspects in recycling lithium-ion batteries: concept of battery identity global passport, Mater. Today 41 (2020) 304–315, https://doi.org/10.1016/j.mattod.2020.09.001.
[4] N. Wu, Y.R. Shi, S.Y. Lang, J.M. Zhou, J.Y. Liang, W. Wang, S.J. Tan, Y.X. Yin, R. Wen, Y.G. Guo, Self-healable solid polymeric electrolytes for stable and flexible lithium metal batteries, Angew. Chem. Int. Ed. 58 (2019) 18146–18149, https://doi.org/10.1002/anie.201910478.
[5] S. Kim, J. Choi, H. Lee, Y.C. Jeong, Y.M. Lee, M.H. Ryou, Suppression of dendrites and granules in surface-patterned Li metal anodes using CsPF6, J. Power Sources 413 (2019) 344–350, https://doi.org/10.1016/j.jpowsour.2018.12.052.

[6] L. Frenck, G.K. Sethi, J.A. Maslyn, N.P. Balsara, Factors that control the formation of dendrites and other morphologies on lithium metal anodes, Front. Energy Res. 7 (2019), https://doi.org/10.3389/fenrg.2019.00115.

[7] D. Cao, X. Sun, Q. Li, A. Natan, P. Xiang, H. Zhu, Lithium dendrite in all-solid-state batteries: growth mechanisms, suppression strategies, and characterizations, Matter 3 (2020) 57–94, https://doi.org/10.1016/j.matt.2020.03.015.

[8] X. Zhang, J.C. Daigle, K. Zaghib, Comprehensive review of polymer architecture for all-solid-state lithium rechargeable batteries, Materials 13 (11) (2020) 2488–2511, https://doi.org/10.3390/ma13112488.

[9] H.J. Kim, T.N.V. Krishna, K. Zeb, V. Rajangam, C.V.V. Muralee Gopi, S. Sambasivam, K.V.G. Raghavendra, I.M. Obaidat, A comprehensive review of li-ion battery materials and their recycling techniques, Electronics (Switzerland) 9 (2020) 1–44, https://doi.org/10.3390/electronics9071161.

[10] J. Duan, X. Tang, H. Dai, Y. Yang, W. Wu, X. Wei, Y. Huang, Building safe lithium-ion batteries for electric vehicles: a review, Electrochem. Energy Rev. 3 (2020) 1–42, https://doi.org/10.1007/s41918-019-00060-4.

[11] X. Huang, R. He, M. Li, M.O.L. Chee, P. Dong, J. Lu, Functionalized separator for next-generation batteries, Mater. Today 41 (2020) 143–155, https://doi.org/10.1016/j.mattod.2020.07.015.

[12] S. Zhao, Q. Wu, W. Ma, L. Yang, Polyethylene oxide-based composites as solid-state polymer electrolytes for lithium metal batteries: a mini review, Front. Chem. 8 (2020), https://doi.org/10.3389/fchem.2020.00640.

[13] Y. Liu, Y. Zhao, W. Lu, L. Sun, L. Lin, M. Zheng, X. Sun, H. Xie, PEO based polymer in plastic crystal electrolytes for room temperature high-voltage lithium metal batteries, Nano Energy 88 (2021) 106250–106259, https://doi.org/10.1016/j.nanoen.2021.106205.

[14] A. Varzi, R. Raccichini, S. Passerini, B. Scrosati, Challenges and prospects of the role of solid electrolytes in the revitalization of lithium metal batteries, J. Mater. Chem. A Mater. 4 (2016) 17251–17259, https://doi.org/10.1039/c6ta07384k.

[15] H.K. Tran, Y.S. Wu, W.C. Chien, S.H. Wu, R. Jose, S.J. Lue, C.C. Yang, Composite polymer electrolytes based on PVA/PAN for all-solid-state lithium metal batteries operated at room temperature, ACS Appl. Energy Mater. 3 (2020) 11024–11035, https://doi.org/10.1021/acsaem.0c02018.

[16] J. Malathi, M. Kumaravadivel, G.M. Brahmanandhan, M. Hema, R. Baskaran, S. Selvasekarapandian, Structural, thermal and electrical properties of PVA-LiCF3SO3 polymer electrolyte, J. Non-Cryst. Solids 356 (2010) 2277–2281, https://doi.org/10.1016/j.jnoncrysol.2010.08.011.

[17] Y. Wang, G. Wang, P. He, J. Hu, J. Jiang, L.Z. Fan, Sandwich structured NASICON-type electrolyte matched with sulfurized polyacrylonitrile cathode for high performance solid-state lithium-sulfur batteries, Chem. Eng. J. 393 (2020) 124705–124712, https://doi.org/10.1016/j.cej.2020.124705.

[18] F. Jiang, X. Wang, X. Fan, H. Zhu, J. Yin, Oxygen-functionalized polyacrylonitrile nanofibers with enhanced performance for lithium-ion storage, ACS Omega 6 (2021) 2542–2548, https://doi.org/10.1021/acsomega.0c04326.

[19] T.N.T. Phan, S. Issa, D. Gigmes, Poly(ethylene oxide)-based block copolymer electrolytes for lithium metal batteries, Polym. Int. 68 (2019) 7–13, https://doi.org/10.1002/pi.5677.

[20] Z. Zeng, V. Murugesan, K.S. Han, X. Jiang, Y. Cao, L. Xiao, X. Ai, H. Yang, J. G. Zhang, M.L. Sushko, J. Liu, Non-flammable electrolytes with high salt-to-solvent ratios for Li-ion and Li-metal batteries, Nat. Energy 3 (2018) 674–681, https://doi.org/10.1038/s41560-018-0196-y.

[21] L. Ye, X. Li, A dynamic stability design strategy for lithium metal solid state batteries, Nature 593 (2021) 218–222, https://doi.org/10.1038/s41586-021-03486-3.

[22] S. Hein, T. Danner, A. Latz, An electrochemical model of lithium plating and stripping in lithium ion batteries, ACS Appl. Energy Mater. 3 (2020) 8519–8531, https://doi.org/10.1021/acsaem.0c01155.

[23] F. Baskoro, H.Q. Wong, H.J. Yen, Strategic structural design of a gel polymer electrolyte toward a high efficiency lithium-ion battery, ACS Appl. Energy Mater. 2 (2019) 3937–3971, https://doi.org/10.1021/acsaem.9b00295.

[24] M. Zhu, J. Wu, Y. Wang, M. Song, L. Long, S.H. Siyal, X. Yang, G. Sui, Recent advances in gel polymer electrolyte for high-performance lithium batteries, J. Energy Chem. 37 (2019) 126–142, https://doi.org/10.1016/j.jechem.2018.12.013.

[25] X. Wu, K. Pan, M. Jia, Y. Ren, H. He, L. Zhang, S. Zhang, Electrolyte for lithium protection: from liquid to solid, Green Energy Environ. 4 (2019) 360–374, https://doi.org/10.1016/j.gee.2019.05.003.

[26] W. Ren, C. Ding, X. Fu, Y. Huang, Advanced gel polymer electrolytes for safe and durable lithium metal batteries: challenges, strategies, and perspectives, Energy Storage Mater. 34 (2021) 515–535, https://doi.org/10.1016/j.ensm.2020.10.018.

[27] X. Cheng, J. Pan, Y. Zhao, M. Liao, H. Peng, Gel polymer electrolytes for electrochemical energy storage, Adv. Energy Mater. 8 (2018), https://doi.org/10.1002/aenm.201702184.

[28] W. Li, Y. Pang, J. Liu, G. Liu, Y. Wang, Y. Xia, A PEO-based gel polymer electrolyte for lithium ion batteries, RSC Adv. 7 (2017) 23494–23501, https://doi.org/10.1039/c7ra02603j.

[29] Y.H. Jo, S. Li, C. Zuo, Y. Zhang, H. Gan, S. Li, L. Yu, D. He, X. Xie, Z. Xue, Self-healing solid polymer electrolyte facilitated by a dynamic cross-linked polymer matrix for lithium-ion batteries, Macromolecules 53 (2020) 1024–1032, https://doi.org/10.1021/acs.macromol.9b02305.

[30] X. Wang, W. Zeng, L. Hong, W. Xu, H. Yang, F. Wang, H. Duan, M. Tang, H. Jiang, Stress-driven lithium dendrite growth mechanism and dendrite mitigation by electroplating on soft substrates, Nat. Energy 3 (2018) 227–235, https://doi.org/10.1038/s41560-018-0104-5.

[31] A.M. Fainleib, O.H. Purikova, Self-healing polymers: approaches of healing and their application, Polym. J. 41 (2019) 4–18, https://doi.org/10.15407/polymerj.41.01.004.

[32] F. Zhao, Q. Sun, C. Yu, S. Zhang, K. Adair, S. Wang, Y. Liu, Y. Zhao, J. Liang, C. Wang, X. Li, X. Li, W. Xia, R. Li, H. Huang, L. Zhang, S. Zhao, S. Lu, X. Sun, Ultrastable anode interface achieved by fluorinating electrolytes for all-solid-state Li metal batteries, ACS Energy Lett. 5 (2020) 1035–1043, https://doi.org/10.1021/acsenergylett.0c00207.

[33] K.R. Reddy, A. El-Zein, D.W. Airey, F. Alonso-Marroquin, P. Schubel, A. Manalo, Self-healing polymers: synthesis methods and applications, Nano-Struct. Nano-Objects 23 (2020) 100500–100521, https://doi.org/10.1016/j.nanoso.2020.100500.

[34] S. Wang, M.W. Urban, Self-healing polymers, Nat. Rev. Mater. 5 (2020) 562–583, https://doi.org/10.1038/s41578-020-0202-4.

[35] H. Wang, P. Wang, Y. Feng, J. Liu, J. Wang, M. Hu, J. Wei, Y. Huang, Recent advances on self-healing materials and batteries, ChemElectroChem. 6 (2019) 1605–1622, https://doi.org/10.1002/celc.201801612.

[36] J. Amici, P. Asinari, E. Ayerbe, P. Barboux, P. Bayle-Guillemaud, R.J. Behm, M. Berecibar, E. Berg, A. Bhowmik, S. Bodoardo, I.E. Castelli, I. Cekic-Laskovic, R. Christensen, S. Clark, R. Diehm, R. Dominko, M. Fichtner, A.A. Franco, A. Grimaud, N. Guillet, M. Hahlin, S. Hartmann, V. Heiries, K. Hermansson, A. Heuer, S. Jana, L. Jabbour, J. Kallo, A. Latz, H. Lorrmann, O.M. Løvvik, S. Lyonnard, M. Meeus, E. Paillard, S. Perraud, T. Placke, C. Punckt, O. Raccurt, J. Ruhland, E. Sheridan, H. Stein, J.-M. Tarascon, V. Trapp, T. Vegge, M. Weil, W. Wenzel, M. Winter, A. Wolf, K. Edström, A roadmap for transforming research to invent the batteries of the future designed within the European large scale research initiative battery 2030+, Adv. Energy Mater. 12 (2022) 2102785–2102827, https://doi.org/10.1002/aenm.202102785.

[37] P. Hundekar, S. Basu, J. Pan, S.F. Bartolucci, S. Narayanan, Z. Yang, N. Koratkar, Exploiting self-heat in a lithium metal battery for dendrite healing, Energy Storage Mater. 20 (2019) 291–298, https://doi.org/10.1016/j.ensm.2019.04.013.

[38] W. Mai, Q. Yu, C. Han, F. Kang, B. Li, Self-healing materials for energy-storage devices, Adv. Funct. Mater. 30 (2020) 1909912–1909943, https://doi.org/10.1002/adfm.201909912.

[39] L. Chen, X. Cai, Z. Sun, B. Zhang, Y. Bao, Z. Liu, D. Han, L. Niu, Self-healing of a covalently cross-linked polymer electrolyte membrane by diels-alder cycloaddition and electrolyte embedding for lithium ion batteries, Polymers (Basel) 13 (23) (2021) 4155–4167, https://doi.org/10.3390/polym13234155.

[40] Y. Sun, Y.Y. Ren, Q. Li, R.W. Shi, Y. Hu, J.N. Guo, Z. Sun, F. Yan, Conductive, stretchable, and self-healing ionic gel based on dynamic covalent bonds and electrostatic interaction, Chin. J. Polym. Sci. 37 (2019) 1053–1059, https://doi.org/10.1007/s10118-019-2325-x.

[41] R. Narayan, C. Laberty-Robert, J. Pelta, J.M. Tarascon, R. Dominko, Self-healing: an emerging technology for next-generation smart batteries, Adv. Energy Mater. 12 (2021) 2102652–2102674, https://doi.org/10.1002/aenm.202102652.

[42] J. Zhang, N. Wang, W. Zhang, S. Fang, Z. Yu, B. Shi, J. Yang, A cycling robust network binder for high performance Si–based negative electrodes for lithium-ion batteries, J. Colloid Interface Sci. 578 (2020) 452–460, https://doi.org/10.1016/j.jcis.2020.06.008.

[43] J. Ryu, S. Kim, J. Kim, S. Park, S. Lee, S. Yoo, J. Kim, N.S. Choi, J.H. Ryu, S. Park, Room-temperature crosslinkable natural polymer binder for high-rate and stable silicon anodes, Adv. Funct. Mater. 30 (2019) 1908433–1908443, https://doi.org/10.1002/adfm.201908433.

[44] T.W. Kwon, Y.K. Jeong, E. Deniz, S.Y. Alqaradawi, J.W. Choi, A. Coskun, Dynamic cross-linking of polymeric binders based on host-guest interactions for silicon anodes in lithium ion batteries, ACS Nano 9 (2015) 11317–11324, https://doi.org/10.1021/acsnano.5b05030.

[45] R. Tamate, K. Hashimoto, T. Horii, M. Hirasawa, X. Li, M. Shibayama, M. Watanabe, Self-healing micellar ion gels based on multiple hydrogen bonding, Adv. Mater. 30 (2018) 1802792–1802799, https://doi.org/10.1002/adma.201802792.

[46] I. Gadwal, A brief overview on preparation of self-healing polymers and coatings via hydrogen bonding interactions, Macromol 1 (2020) 18–36, https://doi.org/10.3390/macromol1010003.

[47] Y.J. Kwon, J.K.R. Modigunta, A.M. Shanmugharaj, H.J. Mun, S.H. Ryu, Synthesis of self-healing polyurethane and its application in graphene/SnO2-pillared carbon anode materials, Polym. Polym. Compos. 28 (2020) 348–355, https://doi.org/10.1177/0967391119879009.

[48] J.H. Yang, J. Lee, S. Lim, S. Jung, S.H. Jang, S. Jang, S.-Y. Kwak, S. Ahn, Y.C. Jung, R.D. Priestley, J.W. Chung, Understanding and controlling the self-healing behavior of 2-ureido-4 [1H]-pyrimidinone-functionalized clustery and dendritic dual dynamic supramolecular network, Polymer (Guildf) 172 (2019) 13–26, https://doi.org/10.1016/j.polymer.2019.03.027.

[49] S.L. Bitsi, M. Stogiou, S. Costanzo, E. Stiakakis, D. Vlassopoulos, A. Nika, M. Chatzichristidi, M. Pitsikalis, Synthesis and characterization of low molar mass end-functionalized homo- and copolymers with ureidopyrimidone, UPy groups, Colloid Polym. Sci. 298 (2020) 637–651, https://doi.org/10.1007/s00396-020-04642-3.

[50] H. Gan, Y. Zhang, S. Li, L. Yu, J. Wang, Z. Xue, Self-healing single-ion conducting polymer electrolyte formed via supramolecular networks for lithium metal batteries, ACS Appl. Energy Mater. 4 (2021) 482–491, https://doi.org/10.1021/acsaem.0c02384.

[51] G. Wang, C. Chen, Y. Chen, X. Kang, C. Yang, F. Wang, Y. Liu, X. Xiong, Self-stabilized and strongly adhesive supramolecular polymer protective layer enables ultrahigh-rate and large-capacity lithium-metal anode, Angew. Chem. 132 (2020) 2071–2076, https://doi.org/10.1002/ange.201913351.

[52] Y.H. Jo, B. Zhou, K. Jiang, S. Li, C. Zuo, H. Gan, D. He, X. Zhou, Z. Xue, Self-healing and shape-memory solid polymer electrolytes with high mechanical strength facilitated by a poly(vinyl alcohol) matrix, Polym. Chem. 10 (2019) 6561–6569, https://doi.org/10.1039/c9py01406c.

[53] K. Yamauchi, J.R. Lizotte, T.E. Long, Thermoreversible poly(alkyl acrylates) consisting of self-complementary multiple hydrogen bonding, Macromolecules 36 (2003) 1083–1088, https://doi.org/10.1021/ma0212801.

[54] B. Liu, Y. Huang, H. Cao, L. Zhao, Y. Huang, A. Song, Y. Lin, X. Li, M. Wang, A novel porous gel polymer electrolyte based on poly(acrylonitrile-polyhedral oligomeric silsesquioxane) with high performances for lithium-ion batteries, J. Membr. Sci. 545 (2018) 140–149, https://doi.org/10.1016/j.memsci.2017.09.077.

[55] B. Zhou, M. Yang, C. Zuo, G. Chen, D. He, X. Zhou, C. Liu, X. Xie, Z. Xue, Flexible, self-healing, and fire-resistant polymer electrolytes fabricated via photopolymerization for all-solid-state lithium metal batteries, ACS Macro Lett. 9 (2020) 525–532, https://doi.org/10.1021/acsmacrolett.9b01024.